Journal of Rock Mechanics and Geotechnical Engineering 14 (2022) 1210–1220

Contents lists available at ScienceDirect

Journal of Rock Mechanics and Geotechnical Engineering

journal homepage: www.jrmge.cn

Full Length Article

Effect of the in situ leaching solution of ion-absorbed rare earth on the mechanical behavior of basement rock

Wen Zhong [a,b], Jian Ouyang [a,c], Daoxue Yang [b,c,*], Xiaojun Wang [a,e], Zhongqun Guo [d,e], Kaijian Hu [a,e]

[a] School of Resources and Environmental Engineering, Jiangxi University of Science and Technology, Ganzhou, 341000, China
[b] State Key Laboratory of Geomechanics and Geotechnical Engineering, Institute of Rock and Soil Mechanics, Chinese Academy of Sciences, Wuhan, 430071, China
[c] Jiangxi Province Key Laboratory of Mining Engineering, Jiangxi University of Science and Technology, Ganzhou, 341000, China
[d] School of Civil and Surveying Engineering, Jiangxi University of Science and Technology, Ganzhou, 341000, China
[e] Key Laboratory of Development and Application of Ionic Rare Earth Resources, Ministry of Education, Ganzhou, 341000, China

ARTICLE INFO

Article history:
Received 18 August 2021
Received in revised form
7 November 2021
Accepted 2 December 2021
Available online 16 December 2021

Keywords:
Leaching solution
Ion-adsorbed rare earth
Mechanical behavior
Soaking duration
Failure pattern

ABSTRACT

A clear understanding of the evolution characteristics of leaching solution's damage to the basement rock of ion-adsorbed rare earth deposits is essential in the in situ leaching mining. In this study, some laboratory tests were carried out to investigate the deterioration behavior and failure mechanism of rock under the erosion of leaching solution. For this purpose, granite specimens were soaked in the leaching solution for different periods and then some physical and mechanical parameters were measured. The experimental results show that the strength of the rock without any soaking is the maximum. After 60 d, the rock strength, mass (dry) and P-wave velocity (dry) decrease to the minimum, while the porosity of the specimens reaches the maximum. Moreover, the failure pattern of the specimens in the uniaxial compression tests is affected as the soaking time increases. The scanning electron microscopy (SEM) image results indicate that the erosion of quartz crystals inside the rock specimens gets more intense with the increase of soaking time. Also, the internal crystal failure mode gradually changes from the trans-granular to the inter-granular. The insights gained from this study are helpful for better understanding the evolution characteristics of leaching solution's damage to the basement rock of ion-adsorbed rare earth deposits.

1. Introduction

Ion-absorbed rare earth ore is the weathering product of granite and other igneous rock containing rare earth hydroxyl water ions. These rare earth ions are adsorbed on the surface of kaolin, illite and other clay minerals during the infiltration of aqueous solution, which results in the formation of ion-absorbed rare earth deposits (Chi and Wang, 1995; Huang et al., 2015; Jha et al., 2016; Wang et al., 2017; Guo et al., 2020). The ion-absorbed rare earth ores are widely distributed in southern China. Rare earth materials are strategic resources of global concern, and are known as the mother of new materials and industrial gold. At present, the ion-absorbed rare earth mines are mainly exploited by the in situ leaching method. A schematic sketch of the leaching mining process is shown in Fig. 1. The erosive effect of the leaching solution of the ion-adsorbed rare earth mining usually results in the basement rock cracking and local collapse of the liquid collection tunnel, which in turn cause the loss of the leaching solution. Therefore, it is essential to study the mechanical deterioration mechanism of the basement rock under the erosion of the leaching solution for the ion-absorbed rare earth mining.

In recent years, extensive research has been conducted to study the effect of water and chemical solutions on the macro-structural, physical and mechanical characteristics of rock materials (Dieterich and Conrad, 1984; Feng et al., 2004; Li et al., 2014, 2019a, 2020a; Miao et al., 2016; Asahina et al., 2018; Hampton et al., 2018; Lin et al., 2019; Shu et al., 2019; Shang et al., 2020; Yu et al., 2020; He et al., 2021). For instance, Xie et al. (2011) analyzed the changes in the mechanical properties of porous limestone materials under

* Corresponding author. State Key Laboratory of Geomechanics and Geotechnical Engineering, Institute of Rock and Soil Mechanics, Chinese Academy of Sciences, Wuhan, 430071, China.
E-mail address: daoxuey@126.com (D. Yang).
Peer review under responsibility of Institute of Rock and Soil Mechanics, Chinese Academy of Sciences.

https://doi.org/10.1016/j.jrmge.2021.12.002

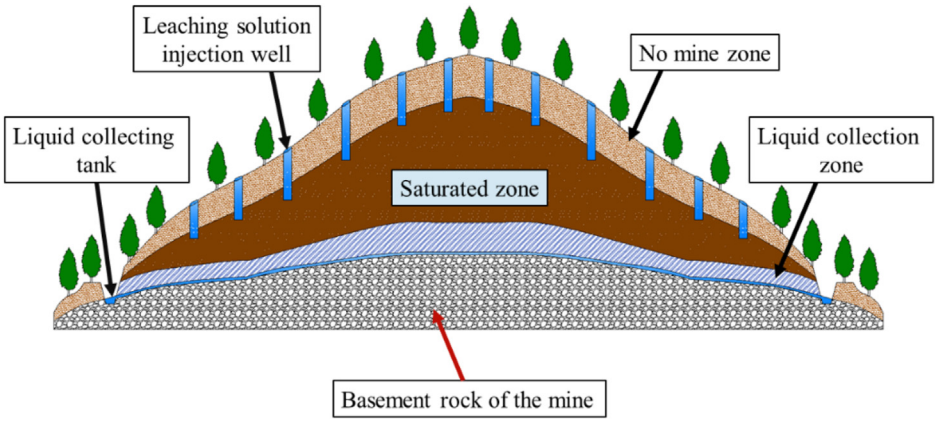

Fig. 1. A schematic sketch of the in situ leaching mining process.

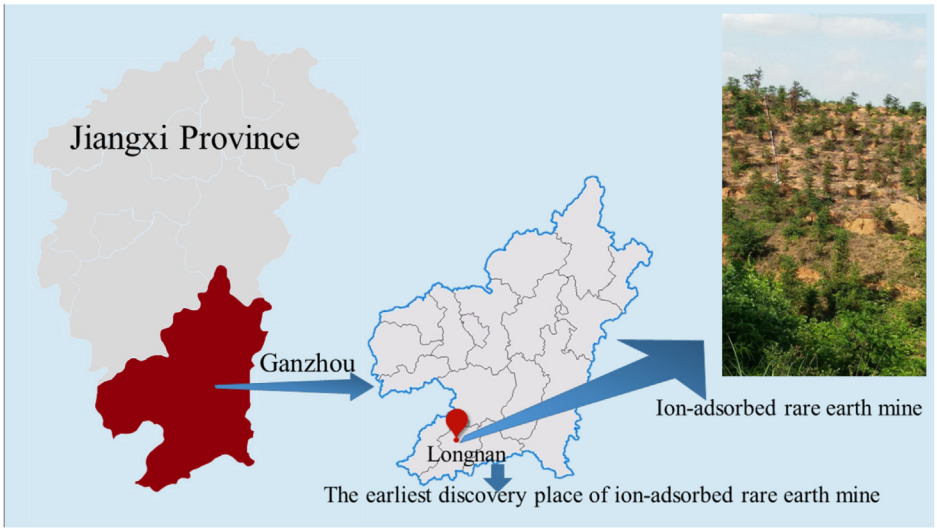

Fig. 2. The sampling site in Longnan ion-adsorbed rare earth mine.

Table 1
Group definitions.

No.	Group	Soaking time (d)	Uniaxial compression test	Average UCS (MPa)
1	C1	0	Yes	115.36
2	C2	30	Yes	93.58
3	C3	60	Yes	84.69
4	C4	90	Yes	102.24
5	C5	120	Yes	96.18
6	SA	Periodical	No	-

Note: UCS denotes the uniaxial compressive strength.

chemical solution erosion. Their experiment results showed that the chemical corrosion resulted in deterioration of the pore collapse limit stress, elastic modulus and cohesion of the rock specimen to some extent. Izadi and Elsworth (2015) studied the permeability characteristics and failure mechanism of rocks under thermo-hydro-mechanical- chemical coupling using FLAC^{3D} models. Li et al. (2019a) analyzed the chemical reaction between the acidic solution and the main diagenetic mineral components inside the sandstone specimen from the perspective of chemical kinetics. Lin et al. (2019) used nuclear magnetic resonance (NMR) technique to analyze the porosity evolution and pore size distribution characteristics of sandstone specimens immersed in chemical solutions with different pH values. They discussed the degradation mechanism of sandstone under the corrosion of acid solution. Shang et al. (2020) conducted direct shear tests on the prefabricated fractured granite specimens under different chemical solutions with different pH values and immersion times. Their results revealed the evolution mechanism of high mineralization, acid, and alkaline groundwater on the short- and long-term mechanical behavior of fractured rock masses in geological engineering. He et al. (2021) analyzed the relations between the water saturation, effective pressure and acoustic velocity by means of multivariate function regression analysis. They indicated that the in situ geophysical properties of rocks could be used to interpret the acoustic wave velocities.

In the recent decades, a large number of studies on mining engineering have been devoted to the study of the microscopic defect structure of rocks under different environmental conditions using different modern techniques such as scanning electron microscopy (SEM), NMR and computed tomography (CT) (Akhtar et al., 2012; Shang et al., 2015; Liu et al., 2016; Saif et al., 2017; Weng et al., 2018; Jin et al., 2019; Li et al., 2019b; Meng et al., 2019; Zhu et al., 2019; Nicco et al., 2020; Tang, 2020; Wong et al., 2020). These modern testing techniques also have been utilized to study the structural evolution characteristics of micro-defects such as micro-cracks and pores during the deterioration of rock materials under the corrosion effect of water and chemical solutions. For

example, Yang et al. (2019) conducted experiments to study the mechanical behavior and evolution characteristics of quartz sandstone under the erosion of HCl, NaCl and NaOH solutions, and distilled water through corrosion-freeze-thaw tests in the laboratory. In that study, SEM technology was used to compare and analyze the morphology and structure of the minerals inside the quartz sandstone under the erosion of different types of chemical solutions. Li et al. (2018) used NMR to study the damage evolution of chemically corroded limestone specimens under cyclic loads. Their research results showed that with the increase of cyclic load, the porosity and micro-crack density of corroded limestone specimens gradually increased. Also, they found that the damage evolution process of the corroded limestone specimens could be divided into micro-crack initiation stage, micro-damage development stage and damage acceleration stage. Cai et al. (2020) used SEM to study the fracture evolution process of sandstone under hydraulic coupling. They demonstrated that the fracture characteristic of sandstone in the dry state was inter-granular fracture within the grains, while that in the saturated state was inter-granular fracture between grains.

Despite the extensive research in this field, the mechanical behavior and deformation mechanism of the basement rock of ion-adsorbed rare earth deposits under the erosion of leaching solution were still not well understood. In this study, some experiments were conducted to investigate the mechanical behavior and deformation mechanism of the basement rock soaked for different periods. In Section 2, the material preparation and the testing procedures were explained. The correlation analysis of mass (dry state), P-wave velocity (dry state), porosity, pH value of leaching solution and uniaxial compression test data, along with the test results of NMR, were discussed in Section 3. Discussion on the experimental results, along with the test results of SEM-EDS, was presented in Section 4.

2. Experiment setup

2.1. Specimen preparation

In this research, some laboratory experiments were conducted to study the erosion effect of the leaching solution on the physical and mechanical parameters of the basement rock of ion-adsorbed rare earth deposits. For this purpose, some granite specimens were collected from an ion-adsorbed rare earth mine located in southern Jiangxi area in China. The location of the sample collection site is indicated in Fig. 2. For laboratory experiments, some cylindrical specimens with the height of 100 mm and the diameter of 50 mm were prepared. The end parallelism of the rock specimen was controlled within ±0.02 mm. The specimen axis was perpendicular to the end faces with a maximum deviation of 0.25 mm. This is the standard specimen geometry for the laboratory experiments as suggested by the International Society for Rock Mechanics (ISRM) (Fairhurst and Hudson, 1999). The mineral composition of the granite specimen was analyzed using X-ray diffraction (XRD) tests. The XRD test results showed that the collected granite specimen was mainly composed of quartz, feldspar, black mica and hornblende. The dry density of the specimen was in the range of 2626–2636 kg/m^3 and its porosity was between 1.16% and 1.18%. It should be noted that the rock specimens with the least variability of P-wave velocity were selected to minimize the data discretization.

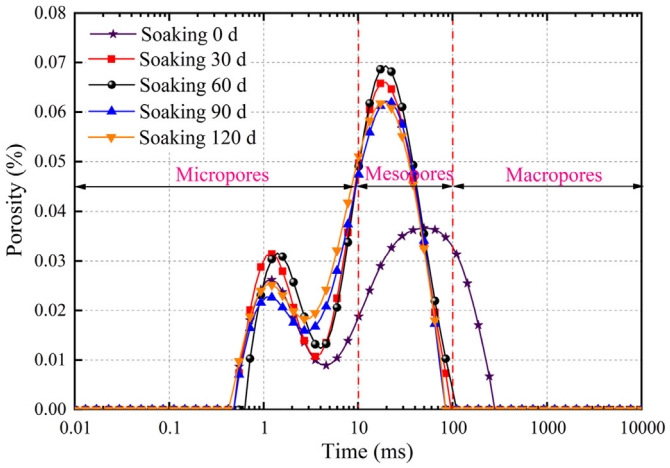

Fig. 4. T_2 spectrum curves and the pore distribution of specimen SA-1 with different soaking durations.

2.2. The leaching solution

The mineralization characteristics of ion-adsorbed rare earth minerals are relatively special, and the rare earth ions are mainly adsorbed on the surface of clay minerals in the form of hydrated ions or hydroxyl hydrated ions. Therefore, many electrolytes can be

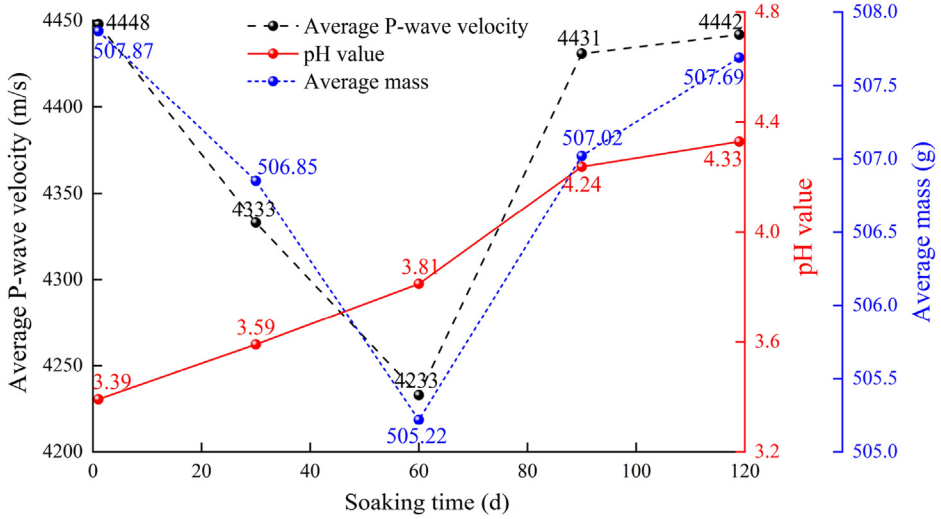

Fig. 3. The average mass and the average P-wave velocity of the specimens and pH value of leaching solution varying with different soaking durations.

selected as the leaching solution (Chi et al., 2005). Considering the cost and efficiency of leaching, most ion-adsorbed rare earth ore extracts the rare earth ions in the ore body by in situ entry and exit methods, and ammonium sulfate solution is generally used as the leaching agent. The leaching equation generally follows the equivalent exchange of ions, and the equation is as follows: Clay-RE^{3+} + $3NH_4^+$ → Clay-$3NH_4^+$ + RE^{3+} (RE^{3+} is a rare earth ion)(-Moldoveanu and Papangelakis, 2012, 2013). The liquid that flows into the collection tunnels after the chemical reaction between the leaching solution and the rare earth components within the ion-adsorbed rare earth deposit is called the leaching solution. The leaching solutions used in this experiment were taken from an ion-adsorbed rare earth mine in southern Jiangxi, which had a pH value of 3.392. The leaching solution was mainly acidic and had an erosive effect on the basement rock. In order to explore the deteriorating effect of leaching solution on the basement rock, the main chemical components of the leaching solution were detected by inductively coupled plasma optical emission spectroscopy test. The major chemical components were NH_4^+, SO_4^{2-}, H^+ and ion-adsorbed rare earth elements. This study uses the leaching solution collected on site to discuss the chemical reaction between it and the basement rock. And then the mechanical response characteristics and deterioration mechanism of the basement rock under the erosion of the leaching solution were revealed.

2.3. Experimental scheme

The prepared rock specimens were divided into six different groups with three specimens in each (Table 1). Five groups of rock specimens were soaked in the leaching solution for different durations of 0 d, 30 d, 60 d, 90 d and 120 d, which were named C1–C5, respectively. It should be noted that for the specimens in group C1, the soaking duration was 0, which means that they were not soaked at all. The specimens in groups C1–C5 were prepared for uniaxial compression tests. The specimens in the 6th group were soaked for 120 d, and this group was named SA. In order to exclude the influence of rock natural micro-defects such as micro-cracks, pores and joints on the experiment results, the specimens in SA were set as the reference, on which only the immersion test was carried out, but no mechanical loading test.

In this study, the mass and P-wave velocity of rock specimens (SA) in dry state and the pH value of leaching solution were measured at different soaking durations of 0 d, 30 d, 60 d, 90 d and 120 d. Moreover, NMR tests were performed on the reference rock specimens (SA) under different soaking durations to study the effect of the immersion duration on the pore distribution characteristics of the rock specimens.

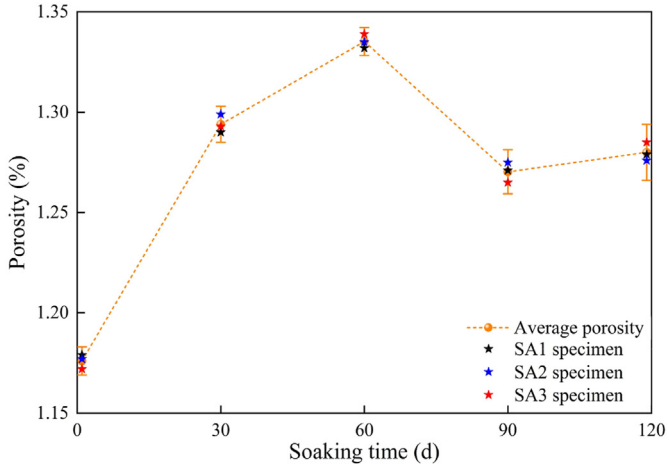

Fig. 5. The average porosity evolution characteristics of rock specimen with different soaking durations.

The uniaxial compression tests were conducted to study the evolutionary characteristics of mechanical behavior of rock specimens with different soaking durations. After removing the rock specimens from the leaching solution, a paraffin wax and a waterproof film were applied to the surface of the specimens to avoid any loss of the leaching solution from the specimens. For this experiment, the rock loading machine and the strain gages were required. The RMT-150C servo-controlled mechanical testing machine developed by the Chinese Academy of Sciences was used to conduct the uniaxial compression tests. The axial and lateral strains during the test were measured by the electrical resistance strain gages. The loading test was carried out using the displacement control method, at a loading rate of 0.001 mm/s. The specimens were continuously loaded until the rock specimens were completely failed.

3. Results and analysis

3.1. Mass and P-wave velocity of specimens and pH value of leaching solution

The reference group (SA) was used to measure the physical properties of the rock specimens at different soaking durations. For this purpose, the reference specimens (SA-1, SA-2 and SA-3) were taken out of the leaching solution and dried, and then their mass and P-wave velocity in the dry state were measured. Also, the pH values of the leaching solution were measured using a MP551 pH/ion concentration measuring instrument. These steps were repeated at 0 d, 30 d, 60 d, 90 d and 120 d of soaking. The relations between the average mass and average P-wave velocity of the specimens in the dry state, and pH values of the leaching solution and the soaking duration are shown in Fig. 3.

Fig. 3 indicates that the average mass of the reference specimens in the dry state decreased by 2.65 g during the soaking duration of 0–60 d and then increased by 2.47 g during the soaking duration of 60–120 d. The figure shows that the average P-wave velocities of the reference specimens in the dry state decreased by 215 m/s during the soaking duration of 0–60 d and then increased by 209 m/s during 60–120 d of soaking. Meanwhile, it can be observed from the figure that the pH value of the leaching solution increased from 3.39 to 4.33 during the experiment (0–120 d of soaking). It implies that the leaching solution had continuous chemical reactions with the rock specimens in the whole soaking duration of 0–120 d. It led to the evolution of micro-defect structure, which in turn resulted in continuous changes in the mass and P-wave velocity of the specimens.

3.2. Effect of the soaking duration on the pore distribution characteristics of the specimens

According to the nuclear magnetic relaxation mechanism, the fluids in different types of pores in the rock have different relaxation times and are distributed in different positions on the T_2 (transverse relaxation time) spectrum curve (Li et al., 2020b). The distribution of the peaks of each nuclear magnetic signal is helpful to determine the development of micro-defects such as cracks, pores and joints in the basement rock. The area of the peak reflects the number of micro-defects in the basement. The width of the peak reflects the distribution of a certain micro-defect structure. The number of peaks reflects the continuity of the pores at each level.

In this study, the NMR technology was utilized to observe and measure the evolution of micro-defects in the specimens. Fig. 4

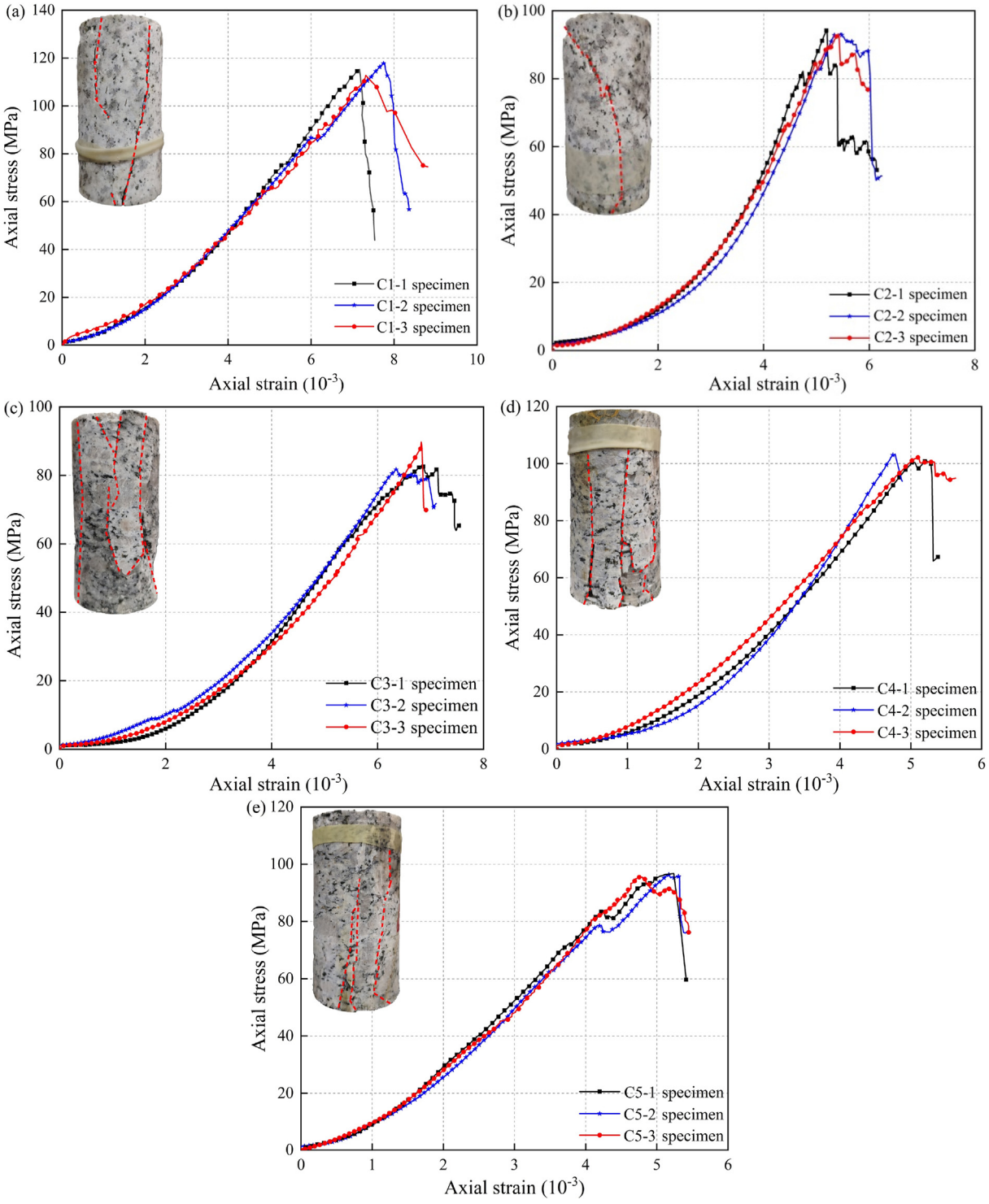

Fig. 6. The stress–strain curves of the specimens with different soaking durations.

shows the T_2 spectrum curves and the pore distribution of SA-1 specimen with different soaking durations. The figure shows that with varying soaking duration, the size and distribution of micro-defect structure inside the specimen change significantly. There were macro-, meso- and micro-pores inside the rock specimens that had not been soaked and the defect structures at various scales had relatively good connectivity. However, only micro- and meso-pores existed inside the rock specimen with 30–120 d of soaking. As the soaking time increased, the peak value of the meso-defect structures increased from 0.0662 to 0.0693 in 30–60 d of soaking duration. It remained almost unchanged, at 0.0312 and 0.0316, in 30–60 d of soaking duration. As the soaking time increased, the peak of the micro-defect structures increased from 0.0229 to 0.0251 in 90–120 d of soaking duration, and it were almost unchanged, at 0.0621 and 0.0619, in 90–120 d of soaking duration.

In order to explore the effect of soaking duration on the porosity of the rock, the porosity of SA specimens was measured under different soaking durations using the NMR technique. The NMR

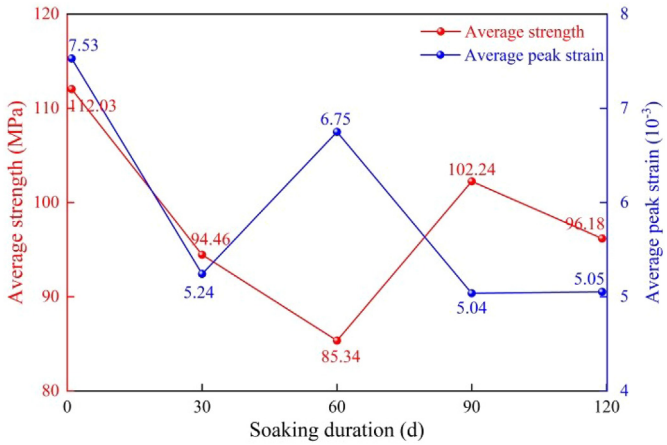

Fig. 7. The average strength and average peak strain of rock specimens with different soaking durations.

analysis results are shown in Fig. 5. The figure implies that the increase of the soaking time resulted in changes in the porosity and average porosity of SA specimens in different periods: (i) an increase by 0.217 in 0–60 d, (ii) a decrease by 0.122 in 60–90 d, and (iii) an increase by 0.009 in 90–120 d.

3.3. Effect of the soaking duration on the stress–strain curve and failure pattern

The stress–strain relation is an important mechanical attribute of rocks, which is essential for studying the elastic and plastic behaviors of rock. The uniaxial compression tests were conducted to investigate the influence of soaking duration on the mechanical behavior of rock specimens with different soaking durations. Fig. 6 shows the stress–strain curves for different specimens. Moreover, the failure patterns of specimens C1-1, C2-1, C3-1, C4-1 and C5-1 are shown in Fig. 6. The figure shows an initial nonlinear (concave) deformation stage in the stress–strain curve of unsoaked specimens (group C1). The elastic deformation stages in the stress–strain curves of C1-1, C1-2 and C1-3 are overlapped, which is an indication of the rock homogeneity.

In Fig. 6, the failure pattern of specimens in C1 is mainly in the forms of tensile and shear fractures. The results show that the failure pattern of specimens in C2 (soaked for 30 d) is dominated by shear fractures, and specimens in C3, C4 and C5 (soaked for 60 d, 90 d and 120 d, respectively) are dominated by tensile fractures. The average strength and average peak strain of the rock specimens with different soaking durations are shown in Fig. 7. In this figure, the average strength of the rock specimens decreased by 26.69 MPa in 0–60 d of soaking, increased by 16.9 MPa in 60–90 d, and decreased by 6.06 MPa in 90–120 d. Furthermore, the average peak strain of the rock specimens indicates a decrease by 2.29×10^{-3} in 0–30 d, an increase by 1.51×10^{-3} in 30–60 d, and a decrease by 1.71×10^{-3} in 60–90 d of soaking duration. The average peak strain of the rock specimens shows no significant changes in 90–120 d of soaking duration.

3.4. Effect of the soaking duration on the characteristic stresses of specimens

According to the stress–strain variation characteristics of the rock specimen under uniaxial compression conditions, the full stress–strain curve of the specimens can be divided into five stages: (i) the crack closure stage, (ii) the linear elastic deformation stage, (iii) the stable crack extension stage, (iv) the unstable crack extension stage, and (v) the post-peak damage stage. The stress levels at each stage are defined as the crack closure stress (σ_{cc}), the crack initiation stress (σ_{ci}), the damage stress (σ_{cd}), and the peak-stress (σ_{ucs}), respectively (Brace, 1964; Bieniawski, 1967; Pan and Lü, 2018; Zhao et al., 2020).

The accurate determination of rock characteristic stresses is of great theoretical and practical significance to rock engineering problems. In recent years, extensive research has been conducted to study the rock characteristic stress classification, and several methods for classification of the crack class have been proposed. Among them, the crack volume strain method (Fig. 8) is the most widely used method (Zhao et al., 2020). In this study, the crack volume strain method was used to investigate the effect of the erosion of the leaching solution on the characteristic stresses of the rock specimens under different soaking time conditions. For this purpose, the average σ_{ci}/σ_{ucs}, σ_{cc}/σ_{ucs} and σ_{cd}/σ_{ucs} of the rock specimens in groups C1–C5 were statistically analyzed using the crack volume strain method (Fig. 9).

From Fig. 9, it can be seen that the average values of σ_{ci}/σ_{ucs}, σ_{cc}/σ_{ucs} and σ_{cd}/σ_{ucs} for the rock specimens soaked for 30 d decreased by 16.19%, 9.62% and 4.62%, respectively, compared to unsoaked rock specimens. The average values of σ_{ci}/σ_{ucs}, σ_{cc}/σ_{ucs} and σ_{cd}/σ_{ucs} for the rock specimens soaked for 90 d increased by 8.46%, 7.18% and 1.97%, respectively, compared to the rock specimens soaked for 30 d. The average values of σ_{ci}/σ_{ucs} and σ_{cc}/σ_{ucs} for the rock specimens soaked for 120 d increased by 4.24% and 2.86%, respectively, while the average σ_{cd}/σ_{ucs} decreased by 2.84%, compared to the rock specimens soaked for 90 d. The above test results show that the immersion time has a significant effect on the characteristic stresses of rock specimens.

4. Discussion

4.1. Changes in SEM images of the specimens

In this study, SEM images were used to study the changes in the mineral composition and cracking of the rock specimens treated with leaching solution for different soaking durations. Fig. 10 shows the SEM images of specimens C1-1, C2-1, C3-1, C4-1 and C5-1. The fracture characteristics of rock specimens treated with leaching solution under different soaking duration conditions are marked in Fig. 10, which are FS1, FS2, FS3, FS4 and FS5, respectively. The fracture surface of the rock specimen without soaking treatment is shown in Fig. 10a. The figure shows that the fracture surface is relatively intact and the crystal particles are closely connected to each other, while the micro-defect structures such as joints, micro-cracks and pores are poorly developed. In the specimen with 30 d of soaking, the fracture surface (Fig. 10b) is rougher than that in the specimen without any leaching treatment, and there are a large number of visible micro-cracks at the fracture surface. The fracture surface of the rock specimen soaked with the leaching solution for 60 d (Fig. 10c) is the roughest with a large number of convex and concave pores. In addition, its pore density is also the highest, which is basically in complete agreement with the pore distribution characteristics of the rock specimen measured by NMR technique. The fracture surface of the rock specimen treated with the leaching solution for 90 d of soaking is shown in Fig. 10d. The figure indicates significant corrosion traces between the crystal particles on the fracture surface. The microstructure becomes unconsolidated and a large number of secondary microcracks are produced on the contact surface of the crystals. Also, fine mineral particles between the micro-cracks can be observed, which result in a relatively poor connectivity. The fracture surface of the rock specimen treated with leaching solution for 120 d of soaking is shown in

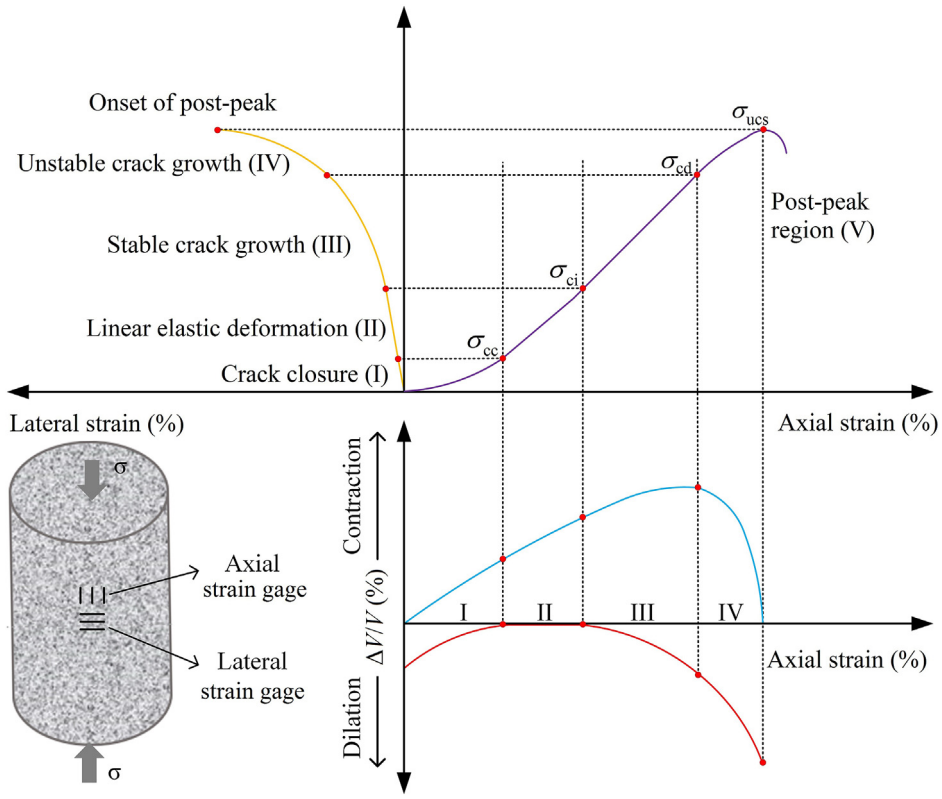

Fig. 8. Stages in the progressive failure of intact rock in compression (modified from Zhao et al., 2020).

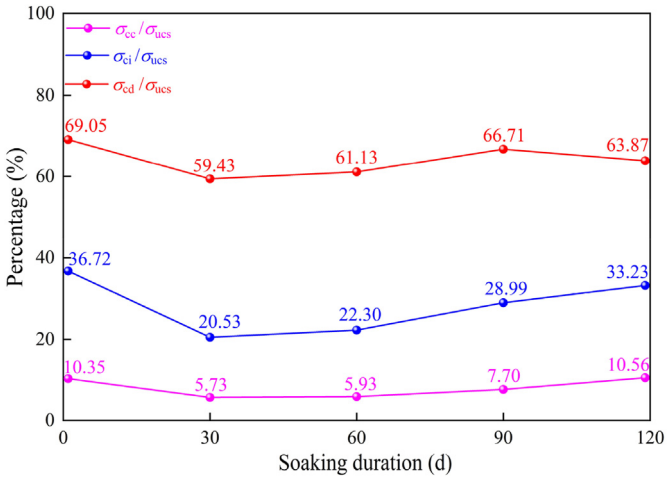

Fig. 9. Effect of the soaking duration on the characteristic stresses.

Fig. 10e. Its internal micro-crack distribution is similar to that in the specimen treated with leaching solution for 90 d.

There are two main failure modes of crystal particles in rock: inter- and trans-granular failures (Zuo et al., 2018; Wu et al., 2019; Tao et al., 2020). In order to explore the influence of leaching solution erosion on rock degradation mechanism, the energy dispersive spectroscopy (EDS) was used to study the form of crystal destruction in rock. EDS is utilized to analyze the mineral composition of the fracture surfaces in the specimens C2-1, C3-1 and C4-1 (Fig. 11). This is helpful to investigate the effect of the leaching solution on the chemical composition of the basement rock of ion-absorbed rare earth deposits. Fig. 11 shows that both sides of the crack of the rock specimen soaked in the leaching solution for 30 d are sodium feldspar. There is no erosion inside the rock specimen, and the main failure type of the internal crystal is trans-granular failure. The internal quartz crystals of the specimen C3-1 (60 d of soaking) are more altered. A large number of silicate crystals are formed, and the main failure mode of the internal crystal is inter-granular failure. After being soaked in the leaching solution for 90 d, the quartz crystal in the rock specimen is altered and $Al_4(SiO_4)_3$ crystals are formed. The main failure mode of the internal crystal is inter-granular failure.

The above test results show that with the increase of the soaking time, the erosion of the quartz crystals inside the rock specimen becomes more intense. Also, the internal crystal failure mode gradually changes from the trans-granular to the inter-granular mode.

4.2. The mechanism of chemical damage to basement rock subjected to leaching solution of ion-absorbed rare earth

Mass is an inherent physical property of rock specimen. Under the erosion action of the leaching solution, some rock-forming mineral components undergo different degrees of chemical decomposition, precipitation and adsorption reactions, resulting in changes in their mass (Houston, 2001; Miao et al., 2016; Huang et al., 2021). The decomposition reaction mainly includes several reactions:

(1) The reaction of oxide with leaching solution:

$$MgO + 2H^+ \rightarrow Mg^{2+} + H_2O$$

$$CaO + 2H^+ \rightarrow Ca^{2+} + H_2O$$

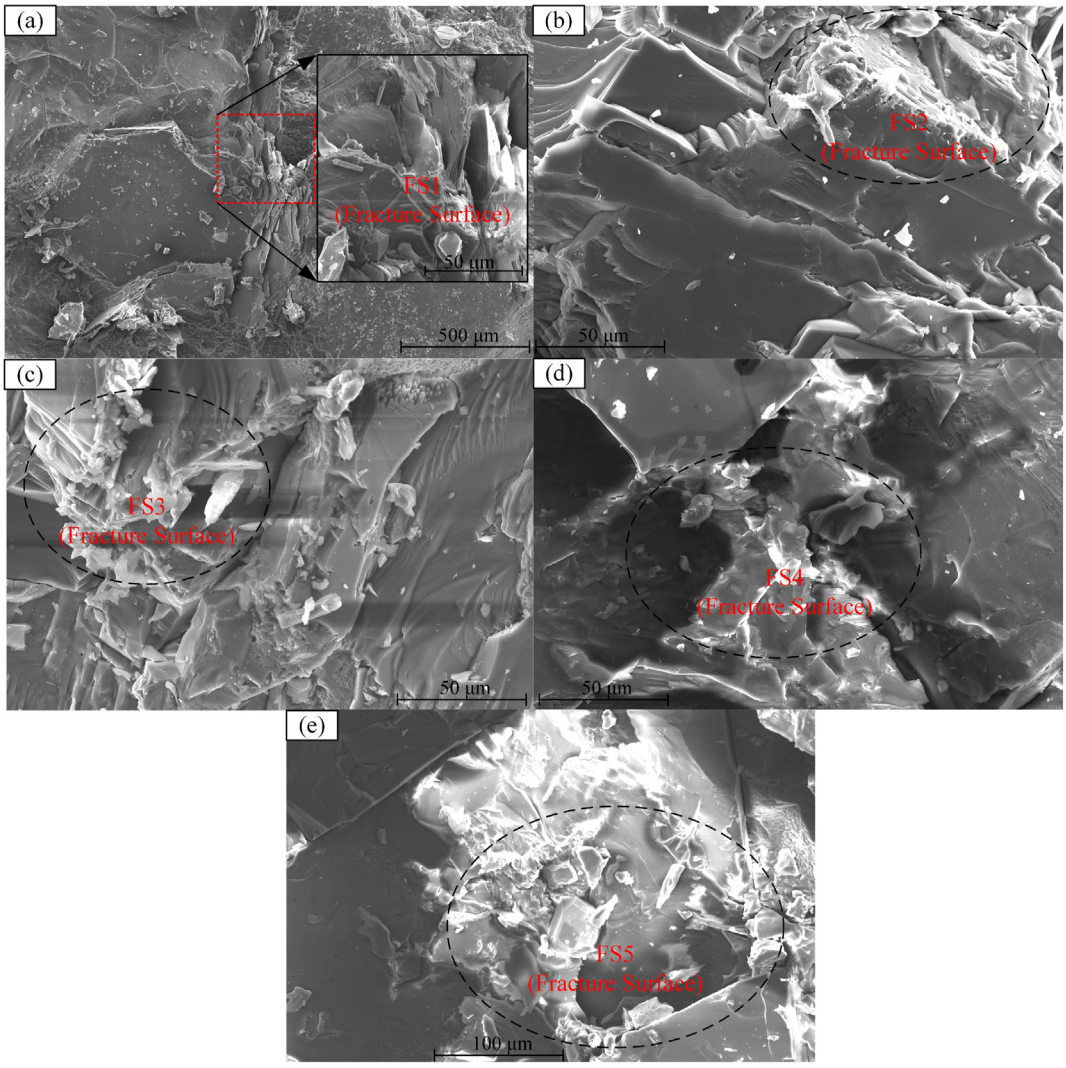

Fig. 10. The SEM images of the specimen after treatment with the leaching solution of ion-absorbed rare earth with different soaking times: (a) 0 d, (b) 30 d, (c) 60 d, (d) 90 d, and (e) 120 d.

$$Al_2O_3 + 6H^+ \rightarrow 2Al^{3+} + 3H_2O$$

$$Fe_2O_3 + 6H^+ \rightarrow 2Fe^{3+} + 3H_2O$$

$$K_2O + 2H^+ \rightarrow 2K^+ + H_2O$$

$$Na_2O + 2H^+ \rightarrow 2Na^+ + H_2O$$

$$SiO_2 + 2H_2O \rightarrow H_4SiO_4$$

(2) The reaction of potash feldspar and albite with leaching solution:

$$NaAlSi_3O_8 + 4H^+ \rightarrow Al^{3+} + 3SiO_2 + 2H_2O + Na^+$$

$$KAlSi_3O_8 + 4H^+ \rightarrow Al^{3+} + 3SiO_2 + 2H_2O + K^+$$

(3) The reaction of calcite with leaching solution:

$$CaCO_3 + 2H^+ \rightarrow Ca^{2+} + H_2O + CO_2\uparrow$$

(4) The reaction of mica with leaching solution:

$$KAl_3Si_3O_{10}(OH)_2 + 10H^+ \rightarrow 3Al^{3+} + 3SiO_2 + 6H_2O + K^+$$

The presence of H^+ in the leaching solution leads to the decomposition reaction of some mineral crystal particles inside the rock specimen. These free ions in the leaching solution chemically react again to produce insoluble substances or colloids adsorbed in the micro-cracks and pores inside the bedrock specimens, which in turn cause the gradual disappearance of the micro-cracks and pores with large size inside the rock specimen. The average mass change (Fig. 3) of specimens SA-1, SA-2 and SA-3 (dry state) under different soaking times and the pore distribution (Fig. 4) measured by NMR tests confirm this speculation. According to the chemical equilibrium principle, when the leaching solution contains a large amount of SO_4^{2-} ions, $CaSO_4$ becomes extremely insoluble, which eventually makes it adsorbed in the form of $CaSO_4 \cdot 2H_2O$ crystals in the internal micro-defect structure of the rock specimen. Therefore, the insoluble substances or colloids adsorbed inside the bedrock specimens mainly include $CaSO_4 \cdot 2H_2O$ crystals and silicate colloids (Fig. 11).

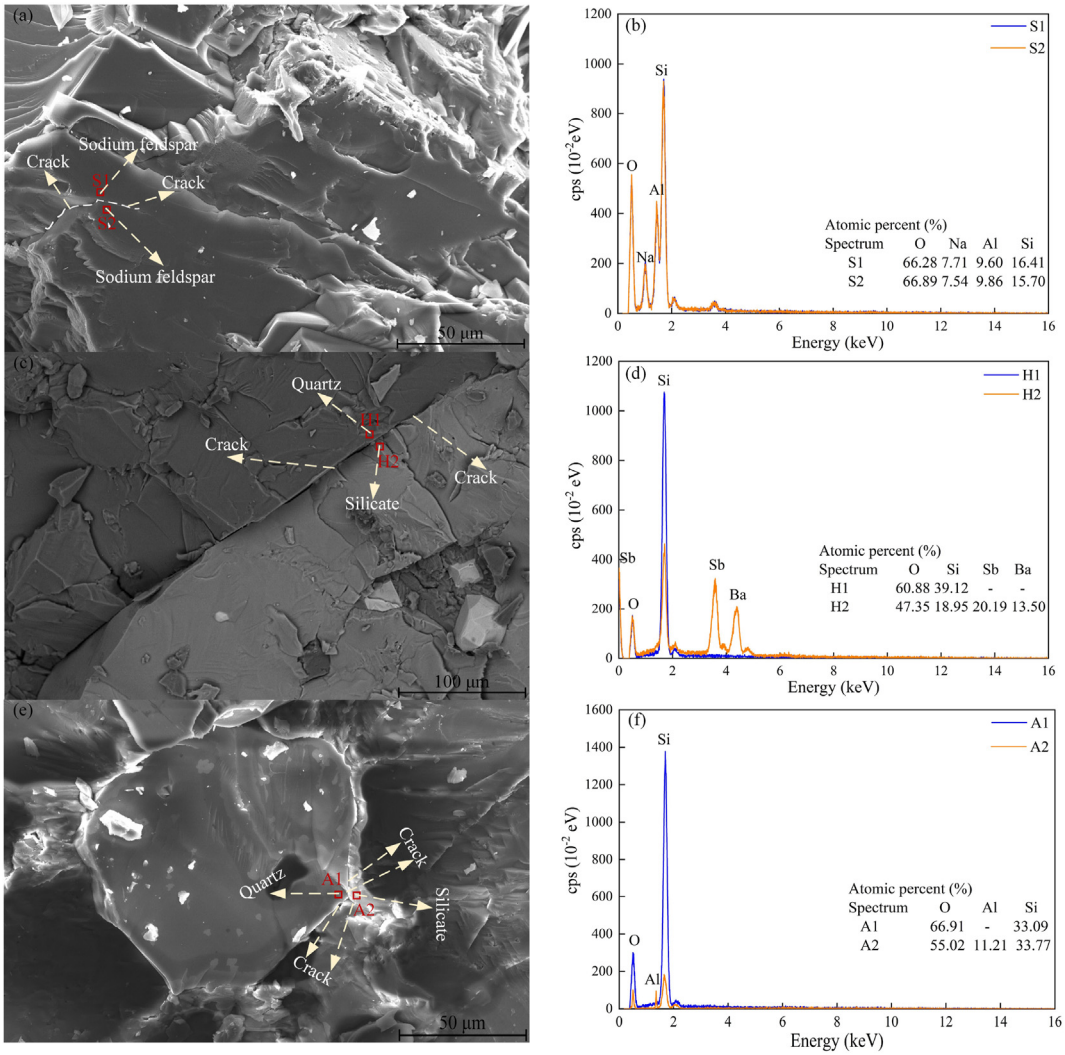

Fig. 11. The SEM images and electron spectroscopy of granite specimens with different soaking times: (a) SEM image of specimen C2-1; (b) Electron spectroscopy of specimen C2-1; (c) SEM image of specimen C3-1; (d) Electron spectroscopy of specimen C3-1; (e) SEM image of specimen C4-1; and (f) Electron spectroscopy of specimen C4-1.

From Fig. 3, it can be seen that in 0–60 d of soaking, the dissolution and separation rates of minerals in the rock specimen are greater than the adsorption rate of mineral precipitation under the erosion of leaching solution. With the increase of immersion time, the porosity of the rock specimen increases, while its mass and strength decrease. In 60–120 d of soaking, the dissolution and separation rates of minerals are less than the adsorption rate of the mineral precipitation under the erosion of leaching solution. The new mineral particles are non-uniformly distributed in the micro-defect structure of the rock specimen, and the large-scale micro-defects are divided into several small size micro-defects. Thus, the porosity of the rock specimen is decreasing in this soaking stage. At the same time, because the newly generated mineral particles block some of the micro-defect structures, many closed micro-defect structures are formed inside the rock specimen. These closed micro-defect structures are filled by the leaching solution. As a result, with the increase of the soaking time in 60–120 d, the mass (dry state) and P-wave velocity of rock specimen increase. Therefore, the phenomenon that the strength of rock specimens soaked for 90 d is greater than that of 60 d is formed.

From Figs. 3, 4 and 6, it can be understood that compared with the pore distribution of specimens in C2 (60 d of soaking), the micro-scale cracks of specimens in C3 (90 d of soaking) increase, and the meso-scale cracks decrease. The results show that a large number of mineral crystal particles are adsorbed in the cracks of rock specimen after being soaked in the leaching solution for 90 d, and these newly formed mineral crystal particles play a supporting role in the process of rock deformation and failure. Compared with the pore distribution of rock specimen treated with leaching solution for 90 d of soaking, the micro-scale cracks of rock specimen treated with leaching solution for 120 d of soaking are further increased. During 120 d of soaking, the pore water pressure inside the rock specimen cannot be ignored. Under the undrained condition, the pore water pressure inside the rock specimen plays a key role in the decrease of the rock strength, which leads to the phenomenon that the strength of the rock specimen soaked for 120 d is less than that of the rock specimen soaked for 90 d.

5. Conclusions

In this study, NMR, SEM, EDS and uniaxial compression tests were conducted on the basement rock specimens that were corroded by leaching solution of ion-absorbed rare earth with different soaking durations. The physical and mechanical

properties (mass, P-wave velocity, porosity, UCS, failure pattern, and characteristic stress points), microstructure characteristics and deterioration mechanism of basement rock after erosion treatment with different soaking durations were systematically examined. Based on the experimental results, the following conclusions can be drawn:

(1) With the increase of the soaking time, the average mass and P-wave velocity of the basement rock specimen in the dry state showed a decreasing and then increasing trend under the erosion effect of the leaching solution, while the pH values of the leaching solution showed a gradually increasing trend. According to the NMR test results, the porosity inside the rock specimen showed an increasing–decreasing trend with the increase of the soaking time. Therefore, it can be inferred that the loss rate of the leaching solution is gradually increasing during 0–60 d of immersion, while the loss rate of the leaching solution is gradually decreasing during 60–120 d of immersion.

(2) With the increase of the soaking time, the failure pattern of rock specimens showed the trend of tension and shear fracture coexisting–shear fracture dominated–tensile fracture dominated. With the increase of soaking time, the strength and peak strain of the rock specimens showed a decreasing–increasing–decreasing trend, but some differences exist in time inflection point. The leaching solution had a significant effect on the rock stresses σ_{ci}/σ_{ucs}, σ_{cc}/σ_{ucs} and σ_{cd}/σ_{ucs}, and all of them were reduced to the minimum value when soaked for 30 d.

(3) With the increase of the soaking time, the erosion of the quartz crystals inside the rock specimens under the erosion of the leaching solution got more intense, and the internal crystal failure mode changed from trans-granular to inter-granular mode. The deterioration mechanism of the mechanical behavior of the rock specimen under the erosion of the leaching solution was revealed by SEM-EDS and NMR techniques from the perspective of corrosion dissolution and precipitation adsorption of the rock-forming mineral components inside the rock.

Declaration of competing interest

The authors declare that they have no known competing financial interests or personal relationships that could have appeared to influence the work reported in this paper.

Acknowledgments

This study was funded by the National Natural Science Foundation of China (Grant No. 51764014), the Natural Science Foundation of Jiangxi Province of China (Grant No. 20192BAB206018), the Education Commission of Jiangxi Province of China (GJJ160674). The authors would also like to thank Dr. Manouchehrian's enthusiastic help, the Youth Jinggang Scholars Program in Jiangxi Province, the Innovative Leading Talents Program in Ganzhou and Chongyi Zhangyuan Tungsten Co. Ltd., China, for the kind supports.

References

Akhtar, F., Andersson, L., Keshavarzi, N., Bergström, L., 2012. Colloidal processing and CO_2 capture performance of sacrificially templated zeolite monoliths. Appl. Energy 97, 289–296.

Asahina, D., Pan, P., Tsusaka, K., Takeda, M., Bolander, J.E., 2018. Simulating hydraulic fracturing processes in laboratory-scale geological media using three-dimensional TOUGH-RBSN. J. Rock Mech. Geotech. Eng. 10 (6), 1102–1111.

Bieniawski, Z.T., 1967. Mechanism of brittle fracture of rock, Part II –Experimental studies. Int. J. Rock Mech. Min. Sci. Geomech. Abstracts 4 (4), 407–423.

Brace, W.F., 1964. State of Stress in the Earth's Crust. Elsevier, New York; USA.

Cai, X., Zhou, Z.L., Zang, H.Z., Song, Z.Z., 2020. Water saturation effects on dynamic behavior and microstructure damage of sandstone: phenomena and mechanisms. Eng. Geol. 276.

Chi, R.A., Tian, J., Li, Z.J., Peng, C., Wu, Y.X., Li, S.R., 2005. Existing state and partitioning of rare earth on weathered ores. J. Rare Earths 23, 756–759.

Chi, R.A., Wang, D.Z., 1995. Rare Earth Extraction Technology. Science Press, Beijing, China (in Chinese).

Dieterich, J.H., Conrad, G., 1984. Effect of humidity on time- and velocity- dependent friction in rocks. J. Geophys. Res. Solid Earth 89, 4196–4202.

Fairhurst, C.E., Hudson, J.A., 1999. Draft ISRM suggested method for the complete stress-strain curve for the intact rock in uniaxial compression. Int. J. Rock Mech. Min. Sci. 36, 279–289.

Feng, X.T., Li, S.J., Chen, S.L., 2004. Effect of water chemical corrosion on strength and cracking characteristics of rocks – a review, 261–263 Key Eng. Mater. 1355–1360.

Guo, Z.Q., Lai, Y.M., Jin, J.F., Zhou, J.R., Sun, Z., Zhao, K., 2020. Effect of particle size and solution leaching on water retention behavior of ion-absorbed rare earth. Geofluids 4921807, 2020.

Hampton, J., Gutierrez, M., Matzar, L., Hu, D., Frash, L., 2018. Acoustic emission characterization of microcracking in laboratory-scale hydraulic fracturing tests. J. Rock Mech. Geotech. Eng. 10 (5), 805–817.

He, W.H., Chen, Z.L., Shi, H.Z., Liu, C.G., Li, S.W., 2021. Prediction of acoustic wave velocities by incorporating effects of water saturation and effective pressure. Eng. Geol. 280, 105890.

Houston, P.L., 2001. Chemical Kinetics and Reaction Dynamics. Mcgraw-Hill Companies, New York, USA.

Huang, X.W., Long, Z.Q., Wang, L.S., Feng, Z.Y., 2015. Technology development for rare earth cleaner hydrometallurgy in China. Rare Met. 34, 215–222.

Huang, Z., Zeng, W., Wu, Y., Li, S.J., Gu, Q.X., Zhao, K., 2021. Effects of temperature and acid solution on the physical and tensile mechanical properties of red sandstones. Environ. Sci. Pollut. Res. Int. 28, 20608–20623.

Izadi, G., Elsworth, D., 2015. The influence of thermal-hydraulic-mechanical- and chemical effects on the evolution of permeability, seismicity and heat production in geothermal reservoirs. Geothermics 53, 385–395.

Jha, M.K., Kumari, A., Panda, R., Rajesh Kumar, J., Yoo, K., Lee, J.Y., 2016. Review on hydrometallurgical recovery of rare earth metals. Hydrometallurgy 165, 2–26.

Jin, X., Wang, X.Q., Yan, W.P., Meng, S.W., Liu, X.D., Jiao, H., 2019. Exploration and casting of large scale microscopic pathways for shale using electrodeposition. Appl. Energy 247, 32–39.

Li, F.B., Sheng, J.C., Zhan, M.L., Xu, L.M., Wu, Q., Jia, C.L., 2014. Evolution of limestone fracture permeability under coupled thermal, hydrological, mechanical, and chemical conditions. J. Hydrodyn. 26, 234–241.

Li, H., Yang, D.M., Zhong, Z.L., Sheng, Y., Liu, X.R., 2018. Experimental investigation on the micro damage evolution of chemical corroded limestone subjected to cyclic loads. Int. J. Fatig. 113, 23–32.

Li, H., Zhong, Z.L., Eshiet, K.I.I., Sheng, Y., Liu, X.R., Yang, D.M., 2019a. Experimental investigation of the permeability and mechanical behaviours of chemically corroded limestone under different unloading conditions. Rock Mech. Rock Eng. 53, 1587–1603.

Li, M., Wang, D.M., Shao, Z.L., 2020a. Experimental study on changes of pore structure and mechanical properties of sandstone after high-temperature treatment using nuclear magnetic resonance. Eng. Geol. 275, 105739.

Li, S.G., Huo, R.K., Yoshiaki, F.J., Ren, D.Z., Song, Z.P., 2019b. Effect of acid-temperature-pressure on the damage characteristics of sandstone. Int. J. Rock Mech. Min. Sci. 122, 104079.

Li, S.G., Wu, Y.M., Huo, R.K., Song, Z.P., Fujii, Y., Shen, Y.J., 2020b. Mechanical properties of acid-corroded sandstone under uniaxial compression. Rock Mech. Rock Eng. 54, 289–302.

Lin, Y., Zhou, K.P., Li, J.L., Ke, B., Gao, R.G., 2019. Weakening laws of mechanical properties of sandstone under the effect of chemical corrosion. Rock Mech. Rock Eng. 53, 1857–1877.

Liu, P., Zhang, D.X., Wang, L.L., Zhou, Y., Pan, T.Y., Lu, X.L., 2016. The structure and pyrolysis product distribution of lignite from different sedimentary environment. Appl. Energy 163, 254–262.

Meng, T., Liu, R.C., Meng, X.X., Zhang, D.H., Hu, Y.Q., 2019. Evolution of the permeability and pore structure of transversely isotropic calcareous sediments subjected to triaxial pressure and high temperature. Eng. Geol. 253, 27–35.

Miao, S.J., Cai, M.F., Guo, Q.F., Wang, P.T., Liang, M.C., 2016. Damage effects and mechanisms in granite treated with acidic chemical solutions. Int. J. Rock Mech. Min. Sci. 88, 77–86.

Moldoveanu, G.A., Papangelakis, V.G., 2012. Recovery of rare earth elements adsorbed on clay minerals: I. Desorption mechanism, 117–118 Hydrometallurgy 71–78.

Moldoveanu, G.A., Papangelakis, V.G., 2013. Recovery of rare earth elements adsorbed on clay minerals: II. Leaching with ammonium sulfate, 131–132 Hydrometallurgy 158–166.

Nicco, M., Holley, E.A., Hartlieb, P., Pfaff, K., 2020. Textural and mineralogical controls on microwave-induced cracking in granites. Rock Mech. Rock Eng. 53, 4745–4765.

Pan, X.H., Lü, Q., 2018. A quantitative strain energy indicator for predicting the failure of laboratory-scale rock samples: application to shale rock. Rock Mech. Rock Eng. 51, 2689–2707.

Saif, T., Lin, Q., Butcher, A.R., Bijeljic, B., Blunt, M.J., 2017. Multi-scale multi-dimensional microstructure imaging of oil shale pyrolysis using X-ray micro-tomography, automated ultra-high resolution SEM, MAPS Mineralogy and FIB-SEM. Appl. Energy 202, 628–647.
Shang, D.L., Zhao, Z.H., Dou, Z.H., Yang, Q., 2020. Shear behaviors of granite fractures immersed in chemical solutions. Eng. Geol. 279, 105869.
Shang, J.L., Hu, J.H., Zhou, K.P., Luo, X.W., Aliyu, M.M., 2015. Porosity increment and strength degradation of low-porosity sedimentary rocks under different loading conditions. Int. J. Rock Mech. Min. Sci. 75, 216–223.
Shu, B., Zhu, R.J., Zhang, S.H., Dick, J., 2019. A qualitative prediction method of new crack-initiation direction during hydraulic fracturing of pre-cracks based on hyperbolic failure envelope. Appl. Energy 248, 185–195.
Tang, H.D., 2020. Multi-scale crack propagation and damage acceleration during uniaxial compression of marble. Int. J. Rock Mech. Min. Sci. 131, 104330.
Tao, R., Sharifzadeh, M., Zhang, Y., Feng, X.T., 2020. Analysis of mafic rocks micro-structure damage and failure process under compression test using quantitative scanning electron microscopy and digital images processing. Eng. Fract. Mech. 231, 107019.
Wang, J.F., Zhu, D.M., Fang, X.H., Qiu, T.S., Liu, Y.B., Zhu, H.L., 2017. Enhanced characteristics and mechanism of static magnetic field on ion-absorbed rare earth precipitation. Int. J. Miner. Process. 158, 13–17.
Weng, L., Wu, Z.J., Li, X.B., 2018. Mesodamage characteristics of rock with a pre-cut opening under combined static–dynamic loads: a nuclear magnetic resonance (NMR) investigation. Rock Mech. Rock Eng. 51, 2339–2354.
Wong, L.N.Y., Zhang, Y.H., Wu, Z.J., 2020. Rock strengthening or weakening upon heating in the mild temperature range? Eng. Geol. 272, 105619.
Wu, X.G., Huang, Z.W., Song, H.Y., Zhang, S.K., Cheng, Z., Li, R., 2019. Variations of physical and mechanical properties of heated granite after rapid cooling with liquid nitrogen. Rock Mech. Rock Eng. 52, 2123–2139.
Xie, S.Y., Shao, J.F., Xu, W.Y., 2011. Influences of chemical degradation on mechanical behaviour of a limestone. Int. J. Rock Mech. Min. Sci. 48, 741–747.
Yang, X.R., Jiang, A.N., Li, M.X., 2019. Experimental investigation of the time-dependent behavior of quartz sandstone and quartzite under the combined effects of chemical erosion and freeze–thaw cycles. Cold Reg. Sci. Technol. 161, 51–62.
Yu, Y.J., Zhu, W.C., Li, L.C., Wei, C.H., Yan, B.X., Li, S., 2020. Multi-fracture interactions during two-phase flow of oil and water in deformable tight sandstone oil reservoirs. J. Rock Mech. Geotech. Eng. 12, 821–849.
Zhao, K., Yang, D., Gong, C., Zhuo, Y., Wang, X., Zhong, W., 2020. Evaluation of internal microcrack evolution in red sandstone based on time–frequency domain characteristics of acoustic emission signals. Constr.Build. Mater. 260, 120435.
Zhu, D., Jing, H.W., Yin, Q., Ding, S.X., Zhang, J.H., 2019. Mechanical characteristics of granite after heating and water-cooling cycles. Rock Mech. Rock Eng. 53, 2015–2025.
Zuo, J.P., Li, Y.L., Zhang, X.Y., Zhao, Z.H., Wang, T.Z., 2018. The effects of thermal treatments on the subcritical crack growth of Pingdingshan sandstone at elevated high temperatures. Rock Mech. Rock Eng. 51, 3439–3454.

Wen Zhong obtained his PhD degree from University of Science and Technology Beijing (USTB), China. He is an associate professor at Jiangxi University of Science and Technology (JXUST), China since 2016. In 2018–2019, he worked at The University of British Columbia (UBC) as a visiting scholar. His research interests include rock and soil mechanics and geohazards in metal mine, efficient development and green extraction of ionic rare earth, and slope stability monitoring and early warning. He has been participated in a number of Chinese national projects regarding the above subjects. He is members of International Society for Rock Mechanics and Rock Engineering (ISRM) and Chinese Society for Rock Mechanics and Engineering (CSRME), and serves as the Secretary-General of the Jiangxi Society for Geotechnical Mechanics and Engineering.